ACS APPLIED MATERIALS & INTERFACES

Research Article

www.acsami.org

Thermoelectric Properties of Indium and Gallium Dually Doped ZnO Thin Films

Nhat Hong Tran Nguyen,[†,‡] Truong Huu Nguyen,[†] Yi-ren Liu,[§] Masoud Aminzare,[§] Anh Tuan Thanh Pham,[†] Sunglae Cho,[∥] Deniz P. Wong,[§] Kuei-Hsien Chen,[§] Tosawat Seetawan,[⊥] Ngoc Kim Pham,[#] Hanh Kieu Thi Ta,[#] Vinh Cao Tran,[†] and Thang Bach Phan*[,†,#]

[†]Laboratory of Advanced Materials, University of Science, Vietnam National University, HoChiMinh City, Vietnam

[‡]Faculty of Applied Science, University of Technology, Vietnam National University, HoChiMinh City, Vietnam

[§]Institute of Atomic and Molecular Sciences, Academia Sinica, Taipei 10617, Taiwan

[∥]Department of Physics, University of Ulsan, Ulsan 13557 Korea

[⊥]Center of Excellence on Alternative Energy, Research Development Institute, Program of Physics, Faculty of Science and Technology, Sakon Nakhon Rajabhat University, 680 Nittayo, Mueang District, Sakon Nakhon, 74000, Thailand

[#]Faculty of Materials Science, University of Science, Vietnam National University, HoChiMinh City, Vietnam

ABSTRACT: We investigated the effect of single and multidopants on the thermoelectrical properties of host ZnO films. Incorporation of the single dopant Ga in the ZnO films improved the conductivity and mobility but lowered the Seebeck coefficient. Dual Ga- and In-doped ZnO thin films show slightly decreased electrical conductivity but improved Seebeck coefficient. The variation of thermoelectric properties is discussed in terms of film crystallinity, which is subject to the dopants' radius. Small amounts of In dopants with a large radius may introduce localized regions in the host film, affecting the thermoelectric properties. Consequently, a 1.5 times increase in power factor, three times reduction in thermal conductivity, and 5-fold enhancement in the figure of merit ZT have been achieved at 110 °C. The results also indicate that the balanced control of both electron and lattice thermal conductivities through dopant selection are necessary to attain low total thermal conductivity.

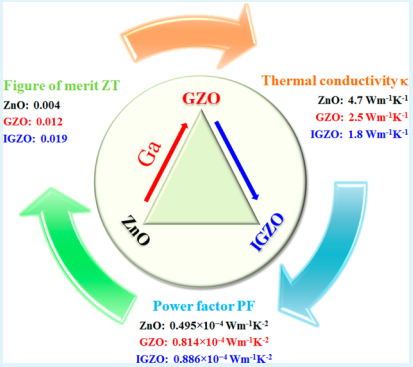

KEYWORDS: *crystalline IGZO thin film, dual doping, Seebeck coefficient, thermal conductivity, localized states*

1. INTRODUCTION

Thermoelectric materials have their ability to directly convert thermal energy to electrical energy without moving parts. Therefore, thermoelectric materials have gained interest due to a requirement for alternative and sustainable energy sources. The performance of thermoelectric materials can be evaluated by the dimensionless figure of merit defined as $ZT = \sigma S^2 T \kappa^{-1}$, where S, σ, and κ are the Seebeck coefficient, electrical conductivity, and thermal conductivity, respectively. Good thermoelectric materials have (1) low thermal conductivity κ for obtaining a large temperature gradient between two ends of the material; (2) high electrical conductivity σ; and (3) a large Seebeck coefficient S is needed to generate a high voltage per unit temperature gradient.[1−8] In general, the simultaneous increase of electrical conductivity and Seebeck coefficient (or power factor $PF = \sigma S^2$) along with a reduction of thermal conductivity are favorable for the enhancement of ZT. However, electrical conductivity and thermal conductivity vary in a similar trend, while the Seebeck coefficient has the exact opposite trend as those of electrical and thermal conductivities. For example, improvement in σ also increases κ and reduces Seebeck coefficient. Therefore, it is difficult to make a pronounced improvement in the power factor $PF = \sigma S^2$ and also the ZT. The thermal conductivity can be reduced by degrading the crystal quality of materials through the introduction of structural defects such as point defects, dislocations, interfaces, precipitates, and nanostructure engineering.[1−8] However, low crystal quality also reduces electrical conductivity. The electrical conductivity can be enhanced by doping. However, the Seebeck coefficient and the electrical conductivity of materials depend on the carrier concentration in a reciprocal way. Harmony control of electrical conductivity, Seebeck coefficient, and thermal conductivity for a high figure of merit through the single doping is critical due to the solubility limitation of the dopant. It seems that dual doping significantly improves the thermoelectric properties better than single doping, especially in ZnO materials. ZnO materials are promising thermoelectric materials since they possess important characteristics: nontoxic, abundant supply, cost-effective, and thermal stability in air in a wide range of temperatures.

Received: August 24, 2016
Accepted: November 18, 2016
Published: November 18, 2016

DOI: 10.1021/acsami.6b10591
ACS Appl. Mater. Interfaces 2016, 8, 33916−33923

Some works reported the improvement of thermoelectric and transport properties of bulk ZnO doped with codopants, such as Al−Mg,[9] Al−Ga,[10] Al−Ti,[11,12] Al−Sm,[11] Al−Ni,[11] Sb−Sn,[12] and Ga−In.[14] Ohtaki et al. reported that the dual doping of ZnO ceramic samples with Al and Ga ($Zn_{1-x-y}Al_xGa_yO$) ceramic samples have the thermoelectric power factor of above 1×10^{-3} $Wm^{-1}K^{-2}$, thermal conductivity below 10 W/mK and thermoelectric figure of merit values ZT of 0.47 at 1000 K.[10] Yamaguchi et al. reported that the thermal conductivity κ values at room temperature of AZO:Ni and AZO:Sm ceramic samples were 9.2 $Wm^{-1}K^{-1}$ and 17.2 $Wm^{-1}K^{-1}$, respectively. The ZT values for AZO:Ni and AZO:Sm at 1073 K reached 0.126 and 0.102, respectively.[11] Park et al. reported that their $Zn_{0.97}Al_{0.02}Ti_{0.01}O$ ceramic samples with the codoping of Al and Ti have a power factor of 3.8×10^{-4} $Wm^{-1}K^{-2}$ at 1073 K.[12] By using different dopants, Park continued to report that the simultaneous Sb- and Sn-added $Zn_{0.985}Sb_{0.005}Sn_{0.01}O$ showed the high thermoelectric power factor (1.15×10^{-3} $Wm^{-1}K^{-2}$) at 1073 K.[13] Recently, Takemoto et al. reported that their $(Ga_{0.002},In_{0.002})Zn_{0.996}O$ sintered sample revealed a high thermoelectric power factor of 6.8×10^{-4} $W^{1-}K^{-2}$, a low lattice thermal conductivity of 1.7 W/mK and a high thermoelectric figure of merit ZT of 0.19 at 773 K.[14]

It is well-known that the thin film technique is another method that can improve the thermoelectric properties of thermoelectric materials because of their stronger quantum confinement effect.

In the case of dual doping of ZnO thin films, Teehan et al. mentioned that dual doping can induce an increase in the density of the states by introducing multiple localized subbands from the impurity materials, which should lead to an increase in Seebeck coefficient S. Then, they reported that their $(ZnO)Al_{.03}In_{.02}$ thin films exhibited the best thermoelectric properties with a power factor of 22.1×10^{-4} Wm^{-1} K^{-2} at a very high temperature of 975 K. However, they did not report the thermal conductivity and figure of merit ZT of (ZnO)-$Al_{.03}In_{.02}$ thin films.[15]

Seo et al. reported the thermoelectric performance of the $InGaO_3(ZnO)_m$ superlattice structure on sapphire substrate. Their single IGZO thin films deposited on sapphire substrate have poor crystallinity and thermoelectric properties due to the large lattice mismatch between IGZO thin film and sapphire substrate. To overcome these advantages, they prepared the $InGaO_3(ZnO)_m$ superlattice structure at high temperatures, in which the ZnO, as a buffer layer, reduces the lattice mismatch with substrate, followed by plasma treatment. Consequently, the PF value of the as-grown, thermally annealed, and plasma treated superlattice samples are 6×10^{-7}, 7×10^{-6}, and 8×10^{-5} Wm^{-1} K^{-2} at 375 K, respectively. The thermal conductivity for the as-grown and thermally annealed superlattice samples were estimated to be 7.53 and 1.00 $Wm^{-1}K^{-1}$, respectively, at room temperature. Since the PF value is low, the $InGaO_3(ZnO)_m$ supperlattice samples still have a low figure of merit ZT although it has low thermal conductivity.[16] Recently, Zheng et al., reported that the power factor of the In-doped AZO thin films shows a a maximum PF value of 2.22×10^{-4} $Wm^{-1}K^{-2}$ at 300 K as the In content increases to 0.71%. However, they do not report the thermal conductivity and figure of merit of their In-doped AZO thin films.[17]

Most of the published literature utilized dual dopants which have either smaller or larger sizes than the Zn^{2+} ion (0.074 nm), such as Al^{3+} (0.053 nm) − Mg^{3+} (0.072 nm) doped ZnO bulk,[9] Al^{3+} (0.053 nm) − Ga^{3+} (0.062 nm) doped ZnO bulk,[10] Al^{3+} (0.053 nm) − Ti^{3+} (0.067 nm) doped ZnO bulk,[11,12] Al^{3+} (0.053 nm) − Ni^{2+} (0.070 nm) doped ZnO bulk,[11] or Sb^{3+} (0.076 nm) − Sn^{2+} (0.118 nm) doped ZnO bulk.[13] Few reports used dual dopants with opposite ion sizes, such as Al^{3+} (0.053 nm) − In^{3+} (0.080 nm) doped ZnO thin films,[15,17] and Ga^{3+} (0.062 nm) − In^{3+} (0.080 nm) doped ZnO superlattice structures.[16]

Compared to those regarding the dual-doped bulk ZnO thermoelectric materials, only a few studies on the thermoelectric property of dual-doped ZnO thin films have been reported. However, the thermal conductivity κ and figure of merit ZT were rarely reported in those published papers.

From our point of view, the miscibility of dopant with ZnO was very poor. Moreover, excessive dopant contents inevitably resulted in a secondary phase, which would deteriorate carrier transport properties. Therefore, using dual dopants, in which one is smaller and the other is larger in size compared to the Zn ion, can be a promising way to harmoniously control crystal quality along with electrical conductivity efficiently and which in turn controls thermoelectric properties. For example, because of differences in the ionic radii between Ga (0.062 nm), In (0.080 nm), and Zn (0.074 nm), a combination of the larger (In) and smaller (Ga) dopants in size compared to the host atom (Zn) can control the ZnO crystal structure more efficiently compared to single dopants.

Here, we reported the first-time creation of thermoelectric Ga and In dual-doped−single crystal ZnO thin film deposited on Si substrate, which has rarely been investigated for use as a thermoelectric material. This research provides useful information on the dual doping effect on the structure and thermoelectric properties (conductivity, Seebeck coefficient, power factor, electron thermal conductivity, lattice thermal conductivity, and figure of merit ZT) of ZnO thin films.

2. EXPERIMENTAL SECTION

ZnO, Ga-doped ZnO (GZO), and In-doped GZO (IGZO) thin films were deposited on Si substrates by magnetron dc-sputtering from ZnO, 5 at% Ga-ZnO, and (0.5 at% In + 4.5 at% Ga)-ZnO homemade targets, respectively. Each target's size is 3 in. in diameter. A Leybold Univex 450 system was used for all depositions. The vacuum chamber was initially evacuated to a base pressure of 6.7×10^{-4} Pa. The sputtering pressure 0.4 Pa was kept constant with a 99.999%-purity Ar flow rate of 20 sccm. The distance of 5 cm between target and substrate and the dc-sputtering power of 60 W were used for all samples. The films ZnO, GZO, and IGZO thin films were deposited at the same substrate temperature of 300 °C. The thin-film thicknesses were about 1100 nm for all films, determined by using a Dektak 6 M stylus profiler and monitored by using a quartz oscillator (XTM/2-INFICON). X-ray diffraction (XRD) patterns for determining the crystal structure of samples were obtained by a D8 Advance−Bruker system using Cu Kα (0.154 nm) spectral line with θ−2θ geometry. The surface morphologies of the films were obtained using field emission scanning electron microscope (FESEM). The elemental analysis was carried out using Energy-dispersive X-ray spectroscopy (EDX), Scanning transmission electron microscopes (STEM), and X-ray photoelectron spectroscopy (XPS).

The electrical conductivity, Seebeck coefficient, and power factor were measured using a commercial apparatus (ZEM-3, ULVAC) under helium atmosphere with a homemade holder for thin film measurement. The carrier type, carrier concentration n, and mobility μ were obtained using a Hall measurement system (HMS-3000, Ecopia using the van der Pauw configuration). The measurements were carried out at different temperatures under argon atmosphere. The temperature-dependent time-domain thermoreflectance (TDTR) technique, which is an ultrafast optical pump−probe metrology, was used to measure thermal conductivity.[18]

DOI: 10.1021/acsami.6b10591
ACS Appl. Mater. Interfaces 2016, 8, 33916−33923

3. RESULTS AND DISCUSSION

Table 1 presents results from EDX measurement of the ZnO, GZO, and IGZO films. The ZnO film is purely composed of Zn and O, and the atomic ratio of Zn to O is 52.57/47.17. The GZO film contains Zn, O and Ga with Zn/O/Ga ≈ 52.91/43.70/2.82 in an atomic ratio. The IGZO film consists of Zn, O, Ga, In, and the Zn/O/Ga/In atomic ratio is 53.45/43.25/2.59/0.33. In the GZO and IGZO films, the atomic weight of Zn atom is lower than that of the Zn in ZnO films, while the atomic weight of the O atom remains unchanged. Therefore, it is expected that dopant elements (Ga, In) could substitute Zn atoms in the host ZnO lattice structure. The dopant concentrations, Ga and In atoms, of the sputtered targets and the deposited films are also different.

Table 1. EDX Mapping Elements of the ZnO, GZO, and IGZO Films

	O K	Zn L	Ga L	In L	Si K	total
ZnO	52.57	47.17			0.26	100
GZO	52.91	43.70	2.82		0.57	100
IGZO	53.45	43.25	2.59	0.33	0.38	100

Figure 1 shows the XPS of Zn 2p, Ga 2p, and In 2p core level spectrum of the ZnO, GZO, and IGZO thin films. Figure 1a–c shows a high symmetry peak of core level of Zn 2p. The binding energy of the Zn $2p_{3/2}$ and Zn $2p_{1/2}$ peaks is located at 1021.9 and 1044.9 eV, respectively, regardless of various doping elements. The binding energies of the Ga $2p_{3/2}$ and Ga $2p_{1/2}$ as seen in Figure 1d–e are found to be 1118.2 and 1145.1 eV, respectively, for both the GZO and IGZO films. The binding energies of the In $2p_{3/2}$ and In $2p_{1/2}$ as shown in Figure 1f are found to be 444.5 and 452.0 eV, respectively. The symmetry peaks give information about the oxidation states of +2, +3, and +3 for Zn, Ga, and In, respectively. This indicates that Ga^{3+} and In^{3+} dopants were incorporated into the host ZnO lattice and had the capacity to successfully substitute the Zn^{2+} ion in the host ZnO lattice.

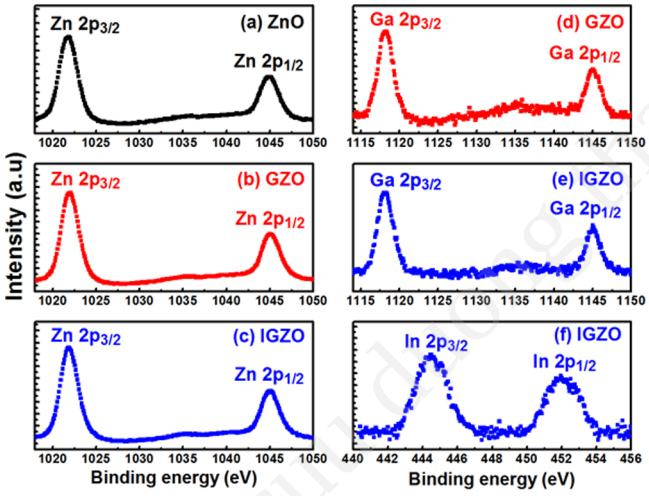

Figure 1. XPS spectrum of the ZnO, GZO, and IGZO films: (a)–(c) Zn 2p, (d, e) Ga 2p, and (f) In 2p.

Figure 2 shows the XPS of O 1s core level spectra of the ZnO, GZO, and IGZO films. The O 1s core level spectra are clearly asymmetric and the peak shapes presented significant differences for the ZnO (two visible peaks) and GZO, IGZO thin films (board peak). The convolution of the O 1s spectrum resulted in three peaks centered at 530 eV, 531.9 and 533.3 eV. The peak at 530 eV (O_I) is assigned to lattice oxygen/stoichiometric phase (O^{2-} ions in wurtzite structure of hexagonal Zn^{2+} ion array). The highest intensity peak at higher binding energy centered at 531.9 eV (O_{II}) is associated with O^{2-} ions in the oxygen-deficient regions with the matrix of the ZnO lattice. The intensity of this component relates to the concentration of oxygen vacancies, which are the source of mobile carrier, in the deposited films. It shows that the concentration of the O_{II} component for the ZnO film is higher than that of the GZO and IGZO films. This indicates that doping reduces the formation on oxygen vacancies. For the ZnO films, the main conductivity is due to the oxygen vacancies and Zn interstitials that donate free electrons to the conduction band. For the GZO and IGZO films, additional free carriers can originate from Ga and In dopants, as well as oxygen vacancies and Zn interstitials, leading to a higher carrier concentration. The lowest intensity peak centered at 533.6 eV (O_{III}) can be attributed to the chemisorbed oxygen impurities as $-CO_3$, adsorbed H_2O or adsorbed O^{2-}.

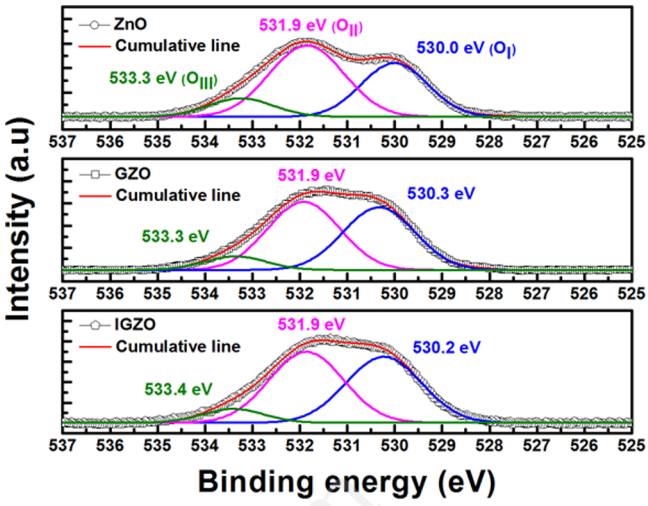

Figure 2. XPS spectrum of O 1s core level of the ZnO, GZO, and IGZO films.

Figure 3a shows the XRD pattern of the deposited films. There was only one strong peak, located at 34.21°, 34.42°, and 34.33° for the ZnO, GZO, and IGZO thin films, respectively. The variation in 2θ value can be due to the different ionic radii of Zn^{2+}, Ga^{3+}, In^{3+}, and also confirm the substitution of Ga^{3+} and In^{3+} ions for Zn^{2+} ions.[19−22] These peaks are assigned the (002) crystalline plane, which is the pronounced diffraction peak of hexagonal wurtzite structure and indicates preferential orientation of the film along *c*-axis perpendicular to the substrate surface.

As shown in detail in Figure 3b, it is noticeable that the number of diffraction peaks and intensity of (002) peak vary with dopant elements. The XRD pattern of the ZnO film shows two additional peaks at 2θ = 31.72° and 36.13° corresponding to (100) and (101) planes, respectively. All of the diffraction peaks are also indexed to the hexagonal wurtzite ZnO structure. The multiple peaks show the polycrystalline nature of the ZnO films with randomly oriented grains. For the GZO films, the (002) peak was significantly increased indicating more favorable of the (002) film orientation. For IGZO films, an

DOI: 10.1021/acsami.6b10591
ACS Appl. Mater. Interfaces 2016, 8, 33916−33923

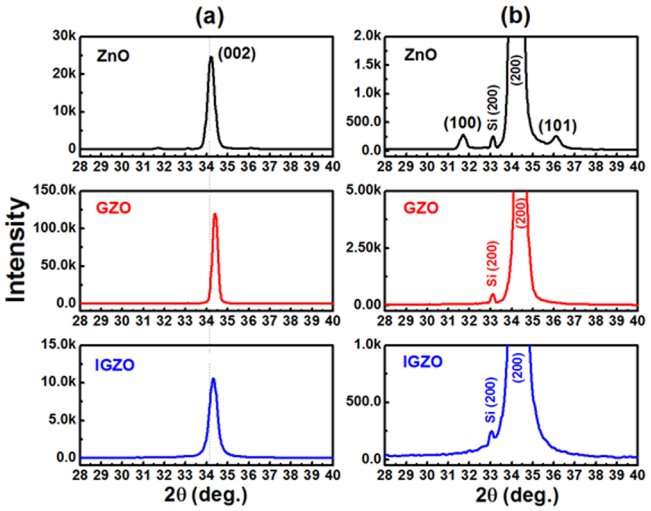

Figure 3. XRD patterns of the ZnO, GZO, and IGZO thin films: (a) full scale and (b) small scale.

additional In dopant reduced the intensity of (002) peak lower than that of ZnO films, indicating that the crystallization of the IGZO thin film had deteriorated. No characteristic diffraction peaks of either Ga_2O_3 or In_2O_3 crystal structures was found.

The calculated value of grain sizes, dislocation densities and lattice constants for the deposited films are listed in Table 2. The grain size D was calculated using the Scherrer formula $D = 0.9\lambda/\beta\cos\theta$, where $\lambda = 0.154$ nm is the X-ray wavelength, β is the full-width at half-maximum (FWHM) of the (002) peak and θ is the Bragg angle. The dislocation density, defined as the length of dislocation lines per unit volume of the crystal, was evaluated from the following relation $\delta = 1/D^2$,[23] where D represents the crystallite size, in order to obtain more information about the amount of defects in the studied thin films. The calculated lattice constant values for ZnO can be expressed as $c_f = 2d_{002} = \lambda/\sin\theta$. A residual stress is generated in the ZnO films because of the differences in the lattice constants and the thermal expansion coefficients between the films and the substrate. The residual stress in the ZnO films can be calculated as follows: $\varepsilon = [2C^2_{13} - C_{33}(C_{11} + C_{12})/2C_{13}] \times [(c_f - c_o)/c_o]$, C_{ij} are the elastic stiffness constants for ZnO (C_{11} = 209.7, C_{33} = 210.9, C_{12} = 121.1, and C_{13} = 105.1 GPa), and c_f and c_o = 0.52 nm are the lattice parameters of the ZnO films and strain-free ZnO bulk, respectively. If the stress is positive, then the biaxial stress will be tensile. However, if the stress is negative, then the biaxial stress will be compressive. The calculated stresses values in the ZnO, GZO, and IGZO films means that all of the deposited films are under compressive stress. Due to lattice mismatch between ZnO and the Si substrate, the undoped ZnO thin films have the largest residual stress and various growth orientations, such as (100), (002), and (101) peaks. The residual stress in the GZO and IGZO thin films are smaller than that of the undoped ZnO thin films due to the difference in ion size between Zn^{2+} (0.074 nm), Ga^{3+} (0.062 nm), and In^{3+} (0.080 nm). Therefore, the two (100) and (101) peaks disappeared in the XRD pattern of the GZO and IGZO thin films.

The FESEM images, which are given in Figure 4, show the influence of dopant elements on the surface morphology and microstructures of the host ZnO films. It can be seen that the surface morphology and microstructure vary with respect to dopant elements. The FESEM image, corresponding to the ZnO film, is composed of visible irregular grains upon a wholly covered surface. The GZO films evidence unclear grain boundaries with flattered surface, while the surface of the IGZO films is less dense. In general, the regular and dense film structures rendered the films with more compact and smoother morphology. This may be due to the highly preferred orientation of the films in the (002) plane. In addition, the STEM elemental mapping indicated that there is the uniform distribution of Ga and In over the host ZnO lattice.

Electrical properties of the ZnO, GZO, and IGZO films are listed in Table 2. Electron concentration n increased from 3.2 × 10^{19} cm^{-3} in pure the ZnO to 65.0 × 10^{19} cm^{-3} in the GZO and then decreased to 42.0 × 10^{19} cm^{-3} in the IGZO thin films. The increase of carrier concentration in the doped ZnO thin films is due to the substitution of Zn^{2+} with Ga^{3+} and In^{3+}, donating one more electron. Since Ga and In dopants have the same valency, replacing a small amount of Ga dopant with In dopant may not make any difference in the electron concentration between the GZO and the IGZO thin films. However, it is also well-known that the electronegativity of In (1.78) is closer to Zn (1.65) than Ga (1.81). The lower electronegativity of In in compared with Ga results in better change of the donating electron. This property would be expected for higher carrier concentrations in the IGZO films than the GZO films. Unfortunately, the Hall measurement show that the GZO film has the highest electron concentration (65 × 10^{19} cm^{-3}) compared to that of the pure ZnO (3.2 × 10^{19} cm^{-3}) and the IGZO thin films (42 × 10^{19} cm^{-3}), even though the dopant concentration (% at Ga = 2.82) in the GZO thin films is smaller than that in the IGZO thin films (% at Ga + In = 2.92), as shown in Table 1. That unexpected result may have originated from the lower crystallinity of IGZO films compared to that of the GZO films, which will be discussed in the following sections.

The electron mobility μ first increased by almost three times from 8.3 $cm^2V^{-1}s^{-1}$ in the pure ZnO to 21.6 $cm^2V^{-1}s^{-1}$ in the GZO thin films and then decreased to 16.5 $cm^2V^{-1}s^{-1}$ in the IGZO thin films. The electron mobility is often associated with electron scattering mechanisms such as scattering by ionized impurities, neutral centers, thermal vibrations of lattice, structural defects (vacancies, dislocation, stacking faults, and residual stress, among others), and grain boundaries. To determine the electron scattering mechanism, we calculated the mean free path (MFP) Λ of electrons using the following formulas: $\Lambda = h(3\pi^2 n)^{1/3}\mu/2\pi e$, where h is the Plank constant, n is the electron density, and μ is the electron mobility.[24]

Table 2. Structural Parameters and Electrical Properties of the ZnO, GZO, and IGZO Thin Films

	2θ (002) (deg)	grain size D (nm)	dislocation density δ (× 10^{-3} nm)	residual stress ε (GPa)	electron density (× 10^{19} cm^{-3})	electron mobility (cm^2/V·s)	resistivity (10^{-2} Ωcm)	mean free path Λ (nm)
ZnO	34.21	21.6	2.14	− 1.5034	3.2	8.3	2.356	0.53
GZO	34.42	27.3	1.34	− 0.1522	65.0	21.6	0.044	3.78
IGZO	34.33	18.8	2.83	− 0.7292	42.0	16.5	0.090	2.48

DOI: 10.1021/acsami.6b10591
ACS Appl. Mater. Interfaces 2016, 8, 33916−33923

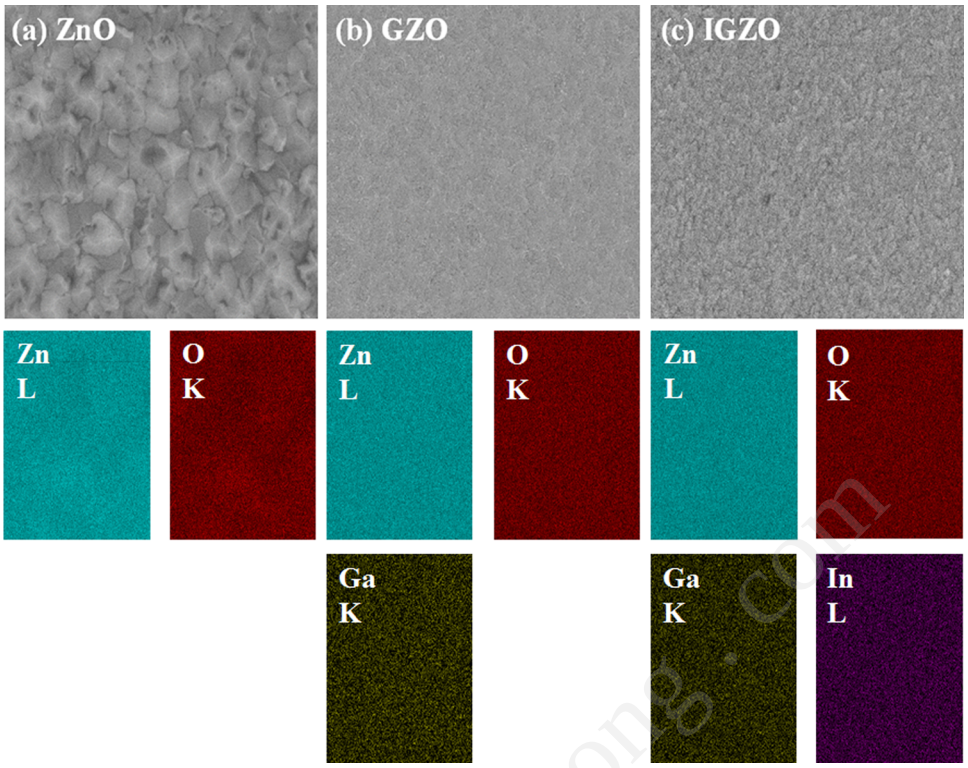

Figure 4. FESEM and STEM mapping of thin films: (a) ZnO, (b) GZO, and (c) IGZO.

Table 2 lists the mean free path (MFP) value of electrons in all deposited films that were examined. It is noted that electron MFP was shorter than the size of the crystalline grain. Consequently, grain boundary scattering is ruled out. Due to the dopants and lattice distortions mentioned above, we suggested that electron mobility is controlled by ionized impurities in grains and lattice distortions. Some works have suggested without any clear explanations that the mobility enhancement may be explained by changes in electronic band structure induced by strain.[25,32] Our results show that the electron mobility varies inversely to the residual stress but proportionally to the carrier concentrations. Therefore, we suggested that both the ionized impurities in grains and lattice distortions might influence the electron mobility of thin films.

Figure 5 shows the conductivity, Seebeck coefficient, and power factor of the ZnO, GZO, and IGZO films, respectively, measured over the temperature range of 30−110 °C.

On the basis of the results, the conductivities of all films are temperature dependent, and its values are consistent with the results recorded from the Hall measurement. The ZnO thin films behaved as semiconductors while both the GZO and IGZO thin films showed typical metallic behavior. Consistent with the Hall results, the GZO thin films have the highest conductivity, and the ZnO thin films have the smallest conductivity.

The Seebeck coefficient *S* value varied differently with films, consistent with the conductivity values: good conducting materials have a low Seebeck coefficient. The *S* value of GZO film is the smallest due to it having the highest conductivity, while the *S* value of ZnO is the largest because it has the lowest conductivity. Among the three films, the *S* value of IGZO film is much smaller than the *S* of pure ZnO film but slightly larger than the *S* of GZO film. Over the entire

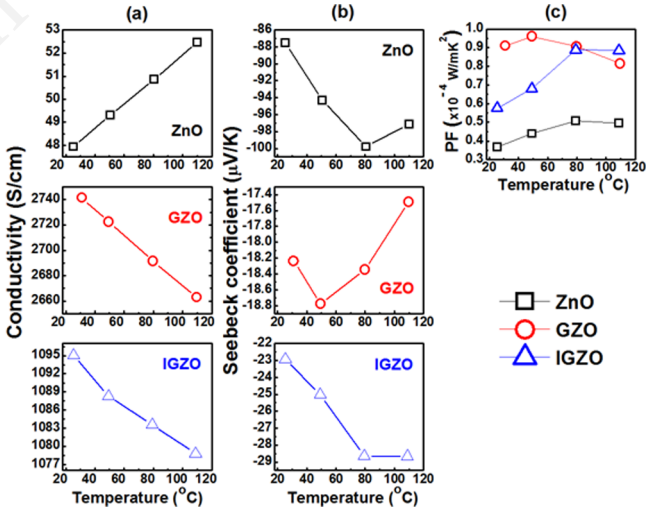

Figure 5. Electrical properties of ZnO, GZO, and IGZO thin films with temperatures: (a) conductivity, (b) Seebeck coefficient, and (c) Power factor PF.

temperature range, the *S* value of GZO is slightly decreased, while the *S* value of both ZnO and IGZO films increased.

It is well-known that the Seebeck coefficient is proportional to the effective mass and inversely proportional to the carrier concentration. Variations of electron concentration and Seebeck coefficient value in the doped GZO and IGZO thin films can be explained through the localization states due to crystal dislocation density, calculated as stated above. The IGZO thin films have largest dopant concentration (Ga + In = 2.92%at) but smaller electron concentrations compared to that of the GZO thin films (Ga = 2.82%at). Because the IGZO thin films have larger localization states (largest crystal dislocation

DOI: 10.1021/acsami.6b10591
ACS Appl. Mater. Interfaces 2016, 8, 33916−33923

density), this may trap some electrons. Hence, incorporation of the dopants causes considerable localization of carriers in the host ZnO lattice and affects the electrical properties, which were reported in some materials such as ITO, Cr-doped $SrTiO_3$, ZnO, and $Mg_{2-\delta}Si_{0.4}Sn_{0.6}$.[26−30] In addition, the Ga and In dopants randomly occupy the Zn sites in the lattice structure. The electronegativity of Ga and In are close but not equal. This difference means that the electrons will experience a fluctuating potential on the atomic cores. This fluctuating potential in the structure can reduce the electron mobility, leading to high effective mass. Consequently, the IGZO thin films have higher Seebeck coefficient than GZO thin films.

The power factor (PF), which represents the electrical contribution to the thermoelectric performance, was calculated from the results in Figure 5a,b. As shown in Figure 5c, the PF of both the ZnO and IGZO films increased while the PF of the GZO decreased over the entire temperature range. The conductivity at 110 °C is 52.46, 2662.78, and 1078.76 S/cm for the pure ZnO, GZO, and IGZO, respectively. The Seebeck coefficient at 110 °C is −97.16, −17.48, and −28.66 μVK^{-1} for the pure ZnO, GZO, and IGZO thin films, respectively. Consequently, the PF values at 110 °C are 0.495×10^{-4}, 0.814×10^{-4} and 0.886×10^{-4} W $m^{-1}K^{-2}$ for the pure ZnO, GZO, and IGZO thin films, respectively. Among the three prepared thin films, the IGZO thin films provide the largest power factor at higher temperatures because of the increase in Seebeck coefficient and conductivity. The PF values are higher when compared to other oxides such as the $InGaO_3(ZnO)_m$ superlattice structure.[16]

Properties of thermal conductivity (electric thermal conductivity κ_e, lattice thermal conductivity $\kappa_{lattice}$, and total thermal conductivity κ_{total}) of the ZnO, GZO, and IGZO films, respectively, measured over the temperature range of 30−110 °C are presented in Figure 6.

We estimated the contribution from the electric thermal conductivity κ_e using the Wiedemann−Franz relation $\kappa_e = L_o T\sigma$, where $L_o = 1/3(\pi k_B/e)$.[14] The observed electric thermal conductivity κ_e (Figure 6a) is consistent with the conductivity as shown in Figure 5a.

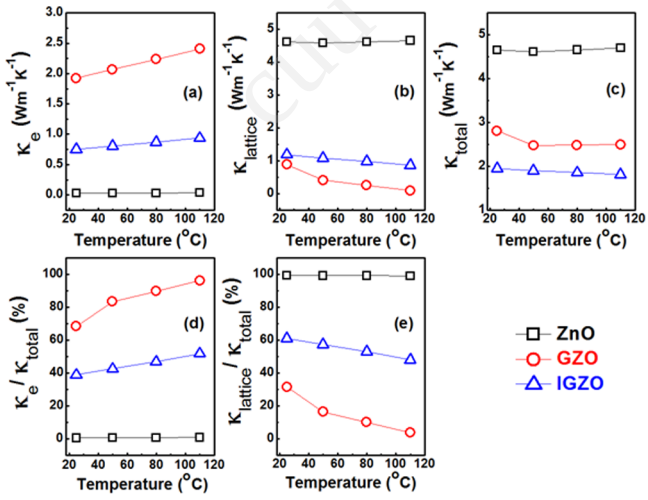

Figure 6. Thermal conductivity of thin films with temperatures: (a) electron thermal conductivity κ_e, (b) lattice thermal conductivity $\kappa_{lattice}$, and (c) total thermal conductivity κ_{total}. Contribution of (d) the electron thermal κ_e and (e) lattice thermal conductivity $\kappa_{lattice}$ to the total thermal conductivity κ_{total}.

The lattice thermal conductivity $\kappa_{lattice}$ (Figure 6b) significantly depends on dopant element. The $\kappa_{lattice}$ values at 110 °C temperature are 4.661, 0.093, and 0.874 $Wm^{-1}K^{-1}$, for undoped ZnO, GZO, and IGZO thin films, respectively. It is noticed that the lattice thermal conductivity $\kappa_{lattice}$ of doped thin films is lower than the $\kappa_{lattice}$ of the undoped ZnO thin films, with the GZO thin films having the lowest $\kappa_{lattice}$. The $\kappa_{lattice}$ of the doped GZO and IGZO thin films decreases monotonically with increasing temperature, suggesting that selective scattering of phonons would be operative in those thin films, such as phonon−phonon scattering. In comparison, the lattice thermal conductivity of our doped GZO and IGZO thin films was lower than that of $(Ga_{0.004},In_{0.004})Zn_{0.992}O$-sintered samples (1.7 $Wm^{-1}K^{-1}$),[14] and Al-doped ZnO nanocomposite samples (2.3 $Wm^{-1}K^{-1}$).[31]

The total thermal conductivity κ_{total} values at 110 °C are 4.7, 2.5, and 1.8 $Wm^{-1}K^{-1}$ for undoped ZnO, GZO, and IGZO thin films, respectively, as shown in Figure 6c. The IGZO thin films have the lowest κ_{total} value over the whole temperature range. It is necessary to calculate the contribution of the electron thermal conductivity κ_e and the lattice thermal conductivity $\kappa_{lattice}$ to the total thermal conductivity κ_{total}, as shown in Figure 6d,e. The reduction of total thermal conductivity κ_{total} becomes a primary and essential task toward improving the ZT of thermoelectric materials. Further, it has been reported that the lattice thermal conductivity $\kappa_{lattice}$ plays a dominant role over the electron thermal conductivity κ_e. However, our results show that the total thermal conductivity of GZO thin films κ_{total} is mainly contributed by the electron thermal conductivity κ_e, while both the electron thermal conductivity κ_e and the lattice thermal conductivity $\kappa_{lattice}$ contribute equally to the total thermal conductivity κ_{total} in the IGZO thin films. In spite of the lowest lattice thermal conductivity, the GZO thin films do not have the lowest total thermal conductivity κ_{total}. These findings suggest that balancing the control of both the electron thermal and lattice thermal conductivities is required in order to obtain good ZT values.

Our IGZO thin films have a total thermal conductivity κ_{total} of 1.8 $Wm^{-1}K^{-1}$, which is smaller than IGZO nanowires (3.3 $Wm^{-1}K^{-1}$),[32] $(Ga_{0.004},In_{0.004})Z_{0.992}O$-sintered samples (2.6 $Wm^{-1}K^{-1}$),[14] Al-doped ZnO thin films (4.89 $Wm^{-1}K^{-1}$),[34] AZO:Ni (9.2 $Wm^{-1}K^{-1}$), and AZO:Sm (17.2 $Wm^{-1}K^{-1}$) ceramic samples,[10] and the as-grown $InGaO_3(ZnO)_m$ superlattice structure (7.53 W/mK).[16] It is noted that the lattice thermal conductivity κ_{total} of our IGZO thin films can be classified into the low level in the ZnO-based thermoelectric materials.

Takemoto et al. concluded that $\kappa_{lattice}$ is attributed mainly to κ_{total} in the $(Ga_{0.004},In_{0.004})Z_{0.992}O$ sintered samples and the formation of three-dimensional stacking faults created in the ZnO by In^{3+} and Ga^{3+} cation doping into the interstitial sites of wurtzite ZnO is effective for the reduction of the lattice thermal conductivity $\kappa_{lattice}$.[14] However, Liang et al. reported the thermoelectric properties of Fe-doped ZnO sintered materials, in which the thermal conductivity generally decreases with the actual Fe content in ZnO lattices (Fe^{3+} cation occupy Zn^{2+} sites), which can be attributed to the point defects introduced into the ZnO lattices and the microstructural refinement (the formation of lamellar $ZnFe_2O_4$ spinel structure).[33] Our GZO thin films have the lowest calculated dislocation density (Table 2) and the lowest lattice thermal conductivity (Figure 6b). The IGZO thin films have the largest calculated dislocation density and higher lattice thermal conductivity. In addition, the

DOI: 10.1021/acsami.6b10591
ACS Appl. Mater. Interfaces 2016, 8, 33916−33923

elemental mapping through STEM, as shown in Figure 4, indicated that there is the uniform spread of Ga and In across the host ZnO lattice. Therefore, no inclusions exist in our IGZO thin films; we suggest that the stacking faults and inclusions might not play an important role in controlling the thermal conductivity of our doped GZO and IGZO thin films.

Since the carrier type in all of the investigated films is the electron, the following defect formation reactions can be considered in undoped ZnO thin films:

$$O_O^x \rightarrow V_O^{\circ\circ} + 2e' + \frac{1}{2}O_2(g) \quad (1)$$

$$V_i^x + Zn(s) \rightarrow Zn_i^{\circ\circ} + 2e' \quad (2)$$

The presence of oxygen vacancies and interstitial zinc donate free electrons in the undoped ZnO thin films.

By doping Ga_2O_3 into the ZnO lattice, the following defect formation reactions can be considered:

$$Ga_2O_3 \xrightarrow{ZnO} 2Ga_{Zn}^{\circ} + V_{Zn}'' + 3O_O^x + 3ZnO \quad (3)$$

Ga^{3+} ions occupy Zn^{2+} ions (Ga_{Zn}°) and create zinc cation vacancy (V_{Zn}'') for the remaining charge neutrality. The electrons donated by Ga^{3+} ions may fully or partially compensate for zinc cation vacancy by giving off no carrier.

$$Ga_2O_3 \xrightarrow{ZnO} 2Ga_{Zn}^{\circ} + 2e' + 2O_O^x + \frac{1}{2}O_2(g) \quad (4)$$

Each Ga^{3+} ion replaces Zn^{2+} ions (Ga_{Zn}°) and donates an electron, enhancing conductivity.

Since the GZO thin films have the largest carrier concentration, reaction 4 is more preferred. It can be explained that the Ga^{3+} ion has a smaller ionic radius compared to that of the Zn^{2+} ion, which minimizes the ZnO lattice dislocations and increases the number of substitutions into Zn^{2+} sites.[22]

Similarity, by doping In_2O_3 into the ZnO lattice, the following defect formation reactions can be considered:

$$In_2O_3 \xrightarrow{ZnO} 2In_{Zn}^{\circ} + V_{Zn}'' + 3O_O^x + 3ZnO \quad (5)$$

$$In_2O_3 \xrightarrow{ZnO} 2In_{Zn}^{\circ} + 2e' + 2O_O^x + \frac{1}{2}O_2(g) \quad (6)$$

However, the IGZO thin films have lower carrier concentration than that of the GZO thin films. Therefore, reactions 4, 5, and 6 exist in the IGZO thin films. Since the In^{3+} ion has a larger ionic radius compared to that of the Zn^{2+} ion, which induces more ZnO lattice dislocations and increases the number of Zn vacancies (V_{Zn}''). Then, V_{Zn}'' compensate the free electrons, lowering the free electron.

The point defects are ($V_O^{\circ\circ}$, $Zn_i^{\circ\circ}$), ($V_O^{\circ\circ}$, $Zn_i^{\circ\circ}$, Ga_{Zn}°) and ($V_O^{\circ\circ}$, $Zn_i^{\circ\circ}$, Ga_{Zn}°, In_{Zn}°, V_{Zn}'') in the undoped ZnO, GZO, and IGZO thin films, respectively. Local compressive strain is developed around the Ga and In ions due to its 3^+ charge. As discussed above relating to the electrical properties, we suggest that the random distribution of Ga and In dopant in the ZnO lattice structures induced these above point defects as localization regions affecting total thermal conductivity.

The thermoelectric figure of merit ZT is calculated according to standard relation $ZT = \sigma S^2 T/\kappa_{total}$ and plotted against temperature, as shown in Figure 7. The ZT value of IGZO thin films increased with increasing temperatures and gave the largest value among three kinds of thin films at 110 °C, ZT = 0.019. Our ZT value is low, but is better than that of the Fe-doped ZnO sintered sample (ZT ≈ 0.005 at 400 °C),[33] Al-doped ZnO pellets (ZT ≈ 0.01 at 600 K),[7] and Al and Ga dual-doped ZnO pellets (ZT ≈ 0.01 at 400 K).[35]

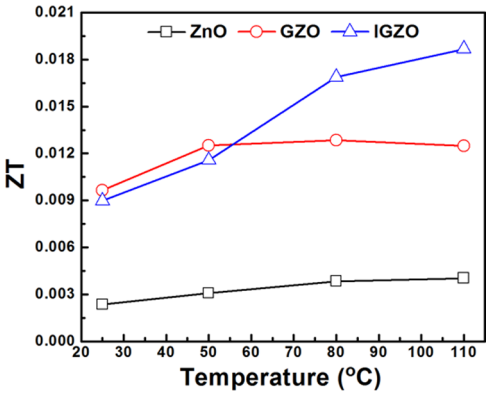

Figure 7. Figure of merit ZT of thin films with temperatures.

4. CONCLUSIONS

The effects of single (Gallium) and multimetal (Gallium and Indium) doping on the crystallinity and thermoelectric properties of sputtered ZnO thin films have been studied systematically. It has been proven that Ga and In elements can be effectively employed to act as donors and also to influence microstructures in the ZnO thin films. The incorporation of Ga in the ZnO films improves their crystalline quality and enables the best electrical properties to be achieved. Incorporation of small amounts of In dopant slightly reduces the crystallinity of the GZO films and improves their thermoelectric properties. Consequently, the power factor PF values at 110 °C are 0.495 × 10^{-4}, 0.814 × 10^{-4}, and 0.886 × 10^{-4} W $m^{-1}K^{-2}$ for the pure ZnO, GZO, and IGZO thin films, respectively. The total thermal conductivity κ_{total} at 110 °C is 4.7, 2.5, and 1.8 $Wm^{-1}K^{-1}$ for the pure ZnO, GZO, and IGZO thin films, respectively. The figure of merit ZT at 110 °C is 0.004, 0.012, and 0.019 for the pure ZnO, GZO, and IGZO thin films, respectively. The improved performance of the IGZO films in comparison with the pure ZnO and GZO thin films may be attributed to the random distribution of In and Ga dopants as point defects, creating localized regions. It is also noted that the total thermal conductivity of GZO thin films is mainly contributed by the electron thermal conductivity κ_e, while both the electron thermal conductivity κ_e and the lattice thermal conductivity $\kappa_{lattice}$ contribute equally into the total thermal conductivity κ_{total} in the IGZO thin films. Our results show that balanced control of both the electron and lattice thermal conductivities through dopants and dopant concentration are important to obtain low thermal conductivity.

AUTHOR INFORMATION

Corresponding Author

*E-mail: pbthang@hcmus.edu.vn (T.B.P).

Notes

The authors declare no competing financial interest.

ACKNOWLEDGMENTS

This work was funded by the National Foundation of Science and Technology Development of Vietnam (NAFOSTED – 103.02-2015.105). The authors gratefully acknowledge Dr.

DOI: 10.1021/acsami.6b10591
ACS Appl. Mater. Interfaces 2016, 8, 33916–33923

Kosuke Watanabe and Prof. Michitaka Ohtaki for supporting STEM elemental analysis (Kyushu University, Japan).

REFERENCES

(1) Ohtaki, M. Recent Aspects of Oxide Thermoelectric Materials for Power Generation from Mid-to-high Temperature Heat Source. *J. Ceram. Soc. Jpn.* **2011**, *119*, 770−775.

(2) Zhao, Y.; Yan, Y.; Kumar, A.; Wang, H.; Porter, W. D.; Priya, S. Thermal Conductivity of Self-assembled Nano-structured ZnO Bulk Ceramics. *J. Appl. Phys.* **2012**, *112*, 034313−034316.

(3) Nong, N. V.; Pryds, N. Nanostructured Oxide Materials and Modules for High-temperature Power Generation from Waste Heat. *Adv. Nat. Sci.: Nanosci. Nanotechnol.* **2013**, *4*, 023002−023008.

(4) Walia, S.; Balendhran, S.; Nili, N.; Zhuiykov, S.; Rosengarten, G.; Wang, Q. H.; Bhaskaran, M. Transition Metal Oxides − Thermoelectric Properties. *Prog. Mater. Sci.* **2013**, *58*, 1443−1489.

(5) Nag, A.; Shubha, V. Oxide Thermoelectric Materials: A Structure−Property Relationship. *J. Electron. Mater.* **2014**, *43* (4), 962−977.

(6) Ren, G.; Lan, J.; Zeng, C. C.; Liu, Y. J.; Zhan, B.; Butt, S.; Lin, Y. H.; Nan, C. W. High Performance Oxides-Based Thermoelectric Materials. *JOM* **2015**, *67* (1), 211−221.

(7) Han, L.; Nong, N. V.; Hung, L. T.; Holgate, T.; Pryds, N.; Ohtaki, M.; Linderoth, S. The Influence of α- and γ-Al_2O_3 Phases on The Thermoelectric Properties of Al-doped ZnO. *J. Alloys Compd.* **2013**, *555*, 291−296.

(8) Han, L.; Nong, N. V.; Zhang, W.; Hung, L. T.; Holgate, T.; Tashiro, K.; Ohtaki, M.; Pryds, N.; Linderoth, S. Effects of Morphology on The Thermoelectric Properties of Al-doped ZnO. *RSC Adv.* **2014**, *4*, 12353−12361.

(9) Tsubota, T.; Ohtaki, M.; Eguchi, K.; Arai, H. Transport Properties and Thermoelectric Performance of $(Zn_{1-y}Mg_y)_{1-x}Al_xO$. *J. Mater. Chem.* **1998**, *8*, 409−412.

(10) Ohtaki, M.; Araki, K.; Yamamoto, K. High Thermoelectric Performance of Dually Doped ZnO Ceramics. *J. Electron. Mater.* **2009**, *38*, 1234−1238.

(11) Yamaguchi, H.; Chonan, Y.; Oda, M.; Komiyama, T.; Aoyama, T.; Sugiyama, S. Thermoelectric Properties of ZnO Ceramics Co-Doped with Al and Transition Metals. *J. Electron. Mater.* **2011**, *40*, 723−727.

(12) Park, K.; Ko, K. Y.; Seo, W. S.; Cho, W. S.; Kim, J. G.; Kim, J. Y. High-temperature Thermoelectric Properties of Polycrystalline $Zn_{1-x-y}Al_xTi_yO$ Ceramics. *J. Eur. Ceram. Soc.* **2007**, *27*, 813−817.

(13) Park, K.; Seong, J. K. Influence of Simultaneous Addition of Sb_2O_3 and SnO_2 on Thermoelectric Properties of $Zn_{1-x-y}Sb_xSn_yO$ Prepared by Tape Casting. *J. Alloys Compd.* **2008**, *464*, 1−5.

(14) Takemoto, H.; Fugane, K.; Yan, P.; Drennan, J.; Saito, M.; Mori, T.; Yamamura, H. Reduction of Thermal Conductivity in Dually Doped ZnO by Design of Three-dimensional Stacking Faults. *RSC Adv.* **2014**, *4*, 2661−2672.

(15) Teehan, S.; Efstathiadis, H.; Haldar, P. Enhanced Power Factor of Indium co-doped ZnO:Al Thin Films Deposited by RF Sputtering for High Temperature Thermoelectrics. *J. Alloys Compd.* **2011**, *509*, 1094−1098.

(16) Seo, D. K.; Shin, S. W.; Cho, H. H.; Kong, B. H.; Whang, D. M.; Cho, H. K. Drastic Improvement of Oxide Thermoelectric Performance Using Thermal and Plasma Treatments of The InGaZnO Thin Film Grown by Sputtering. *Acta Mater.* **2011**, *59*, 6743−6750.

(17) Zheng, Z. H.; Fan, P.; Luo, J. T.; Liang, G. X.; Zhang, D. P. Enhanced room-temperature Thermoelectric Performance of In-doped ZnO:Al Thin Films Through The Prefabricated Layer Doping Method. *Electron. Mater. Lett.* **2015**, *11* (3), 429−434.

(18) Zhu, J.; Tang, D.; Wang, W.; Liu, J.; Holub, K. W.; Yang, R. Ultrafast Thermoreflectance Techniques for Measuring Thermal Conductivity and Interface Thermal Conductance of Thin Films. *J. Appl. Phys.* **2010**, *108*, 094315.

(19) Kim, K. H.; Park, K. C.; Ma, D. Y. Structural, Electrical and Optical Properties of Aluminum Doped Zinc Oxide Films Prepared by Radio Frequency Magnetron Sputtering. *J. Appl. Phys.* **1997**, *81*, 7764.

(20) Asmar, R. A.; Juillaguet, S.; Ramonda, M.; Giani, A.; Combette, P.; Khoury, A.; Foucaran, A. Fabrication and Characterization of High Quality Undoped and Ga_2O_3-doped ZnO Thin Films by Reactive Electron Beam Co-evaporation Technique. *J. Cryst. Growth* **2005**, *275*, 512−520.

(21) Lin, P. F.; Ko, C. Y.; Lin, W. T.; Lee, C. T. Effects of Processing Parameters on Ultraviolet Emission of In-doped ZnO Nanodisks Grown by Carbothermal Reduction. *Mater. Lett.* **2007**, *61*, 1767−1770.

(22) Sim, K. U.; Shin, S. W.; Moholkar, A. V.; Yun, J. H.; Moon, J. H.; Kim, J. H. Effects of Dopant (Al, Ga, and In) on The Characteristics of ZnO Thin Films Prepared by RF Magnetron Sputtering System. *Curr. Appl. Phys.* **2010**, *10*, S463−S457.

(23) Kose, S.; Atay, F.; Bilgin, V.; Akyuz, I. In Doped CdO Films: Electrical, Optical, Structural and Surface Properties. *Int. J. Hydrogen Energy* **2009**, *34*, 5260−5266.

(24) Pham, D. P.; Nguyen, H. T.; Phan, B. T.; Hoang, V. D.; Maenosono, S.; Tran, C. V. Influence of Addition of Indium and Post-annealing on Structural, Electrical and Optical Properties of Gallium-doped Zinc Oxide Thin Films Deposited by Direct-current Magnetron Sputtering. *Thin Solid Films* **2015**, *583*, 201−204.

(25) Chen, D. S.; Zhao, Y.; Chen, Y.; Wang, B.; Chen, H. Y.; Zhou, J.; Liang, Z. Q. One-Step Chemical Synthesis of ZnO/Graphene Oxide Molecular Hybrids for High-Temperature Thermoelectric Applications. *ACS Appl. Mater. Interfaces* **2015**, *7* (5), 3224−3230.

(26) Amrani, A. E.; Hijazi, F.; Lucas, B.; Boucle, J.; Aldissi, M. Electronic Transport and Optical Properties of Thin Oxide Films. *Thin Solid Films* **2010**, *518* (16), 4582−4585.

(27) Irimia, M.; Iacomi, F.; Rambu, A. P.; Sandu, A. V.; Doroftei, C.; Sandu, I. Influence of Substrate Temperature on the Properties of Ga-Doped ZnO thin Films. *Rev. Chim (Bucharest).* **2012**, *63* (8), 803−808.

(28) Phan, B. T.; Lee, J. Effects of Interfacial Oxygen-deficient Layer on Resistance Switching in Cr-doped SrTiO3 Thin Films. *Appl. Phys. Lett.* **2008**, *93*, 222906−222913.

(29) Phan, B. T.; Lee, J. Nonadiabatic Small Polaron Tunneling Conduction in Reduced Cr-doped $SrTiO_{3-\delta}$ Thin Films. *Appl. Phys. Lett.* **2009**, *94*, 232102−232103.

(30) Zhang, L.; Xiao, P.; Shi, L.; Henkelman, G.; Goodenough, J. B.; Zhou, J. S. Localized Mg-vacancy States in The Thermoelectric Material $Mg_{2-\delta}Si_{0.4}Sn_{0.6}$. *J. Appl. Phys.* **2016**, *119*, 085104.

(31) Jood, P.; Mehta, R. J.; Zhang, Y.; Peleckis, G.; Wang, X.; Siegel, R. W.; Borca-Tasciuc, T.; Dou, S. H.; Ramanath, G. Al-Doped Zinc Oxide Nanocomposite with Enhanced Thermoelectric Properties. *Nano Lett.* **2011**, *11*, 4337−4342.

(32) Andrews, S. C.; Fardy, M. A.; Moore, M. C.; Aloni, S.; Zhang, M.; Radmilovic, V.; Yang, P. Atomic-level Control of The Thermoelectric Properties in Polytypoid Nanowires. *Chem. Sci.* **2011**, *2*, 706−714.

(33) Liang, X. Thermoelectric Transport Properties of Fe-Enriched ZnO with High-Temperature Nanostructure Refinement. *ACS Appl. Mater. Interfaces* **2015**, *7*, 7927−7937.

(34) Saini, S.; Mele, P.; Honda, H.; Henry, D. J.; Hopkins, P. E.; Molina-Luna, L.; Matsumoto, K.; Miyazaki, K.; Ichinose, A. Enhanced Thermoelectric Performance of Al-doped ZnO Thin Films on Amorphous Substrate. *Jpn. J. Appl. Phys.* **2014**, *53*, 060306−060314.

(35) Han, L.; Hung, L. T.; Nong, N. V.; Pryds, N.; Linderoth, S. The Influence of Spark Plasma Sintering Temperature on The Microstructure and Thermoelectric Properties of Al,Ga Dual-Doped ZnO. *J. Electron. Mater.* **2013**, *42* (7), 1573−1581.

DOI: 10.1021/acsami.6b10591
ACS Appl. Mater. Interfaces 2016, 8, 33916−33923